Effect of Micropore Topology on the Structure and Properties of Zeolite Polymer Replicas

Stacy A. Johnson, Elaine S. Brigham,† Patricia J. Ollivier, and Thomas E. Mallouk*

Department of Chemistry, The Pennsylvania State University, University Park, Pennsylvania 16802

Received May 7, 1997. Revised Manuscript Received September 10, 1997⊗

Zeolites were used as templates to prepare microporous polymer replicas. Phenol−formaldehyde polymers were synthesized and cured within the channel networks of zeolites Y, β, and L. Dissolution of the aluminosilicate framework in aqueous HF yields an organic replica that contains <2% aluminosilicate. The zeolite template exerts important topological effects on the structure and physical properties of the replica. Using zeolites Y and β, which have three-dimensionally interconnected channel structures, the microporosity of the template is reflected in the replica polymer. Pore size distributions are consistent with the predominance of 5−6 Å walls in the parent zeolite. In contrast, complete collapse of the replica, to a give nonporous material, occurs upon removal of the zeolite L template, since the latter has a one-dimensional channel structure. TEM and SEM micrographs also show evidence of collapse in the latter case. Pyrolysis of the zeolite−resin composites at 900 °C, and subsequent etching, produces very high surface area, electronically conducting replicas. Under these conditions the zeolite Y replica has markedly lower conductivity than those obtained from β and L, which have straight channels.

Introduction

The synthesis of new micro- and mesoporous materials is interesting for both practical and fundamental reasons. Many of the desirable properties of these materials stem from the fact that the dimensions of their pores are similar to those of molecules and supramolecular aggregates (3−100 Å). The size distribution and topology of micropores in materials of similar compositions can be very different, depending on the method of synthesis. Very high surface areas can arise from textural irregularities on the surface of an amorphous solid (e.g., silica gel), from spaces between platelike sheets of layered compounds (e.g., pillared clays, high surface area carbons), or from the regular open frameworks of crystalline materials (e.g., zeolites and mesoporous molecular sieves). While in the first two examples there is structural disorder and consequently a distribution of pore sizes, in the third case the distribution is narrow and the topology of interconnections is well-defined. The size and shape selectivity of the latter materials makes them useful for several important technological processes, including ion exchange, separations, catalysis, chemical sensing, and host−guest chemistry.

Zeolites and related molecular sieves are typically made by hydrothermal (or solvothermal) methods. While there is now quite a bit of variety in their composition, they are still limited to materials (oxides, chalcogenides, phosphates, etc.) that can be processed in this manner. However, if porous inorganic frameworks are themselves used as synthesis templates, a different set of compositions (polymers, covalent semiconductors, metals, and so on) becomes accessible via replication. Replication—the process of filling the external and/or internal pores of a solid with a different material, and physically or chemically separating the resulting material from the "mold" or "master"—is a technique that is widely used in microscopy and printing. Replica polymers, metals, and semiconductors have been prepared from solids with pores on the length scale of nanometers to microns. These template materials have included nanoporous membranes, anodic alumina, and clays.[1−7] Various imprinted polymers that retain the size and shape memory of small-molecule templates have also been reported.[8−10] However, none of these techniques produces a three-dimensional microporous material.

Zeolites represent an interesting and extreme test case for replication strategies, because the dimensions of their cages and channels are quite similar to those of the organic molecules that constitute the replica. Several groups have made preliminary studies of this problem. Enzel and Bein studied the effects of a zeolite Y host on the preparation and properties of poly(acrylonitrile).[11] Similar reactions were recently used to prepare porous carbon replicas of zeolite Y with

† Current address: Union Carbide Corporation, South Charleston, WV 25303.

⊗ Abstract published in *Advance ACS Abstracts,* November 1, 1997.

(1) (a) Wu, C.-G.; Bein, T. *Science* **1994**, *266*, 1013. (b) Wu, C.-G.; Bein, T. *Science* **1994**, *264*, 1757.
(2) Blatter, F.; Schumacher, E. *Surf. Sci* . **1988**, *203*, 571.
(3) Bandosz, T. J.; et al. *Chem. Mater.* **1996**, *8*, 2023.
(4) (a) Kyotani, T., Sobobe, N.; Tomita, A. *Nature* **1988**, *331*, 331. (b) Sonobe, N., Kyotani, T.; Tomita, A. *Carbon* **1988**, *4*, 573. (c) Sonobe, N., Kyotani, T., Hishiyama, Y., Shiraishi, M., and Tomita, A. *J. Phys. Chem.* **1988**, *92*, 2, 7029. (d) Kyotani, T., Sobobe, N.; Tomita, A. *Carbon* **1990**, *4*, 483. (e) Kyotani, T., Sobobe, N.; Tomita, A. *Carbon* **1991**, *29*, 9, 61. (f) Kyotani, T., Yamada, H., Sonobe, N.; Tomita A. *Carbon* **1994**, *32*, 2, 627. (g) Kyotani, T., Mori, T.; Tomita, A. *Chem. Mater.* **1994**, *6*, 2138.
(5) Masuda, H.; Fukuda, K. *Science* **1995**, *268*, 1466.
(6) (a) Weber, J. N., White, E. W.; Lebiedzik, J. *Nature* **1971**, *233*, 337. (b) White, R. L.; Weber, J. N.; White, E. W. *Science* **1972**, *176*, 1922. (c) Roy, D. M.; Linnehan, S. K. *Nature* **1974**, *247*, 220.

S0897-4756(97)00327-X CCC: $14.00

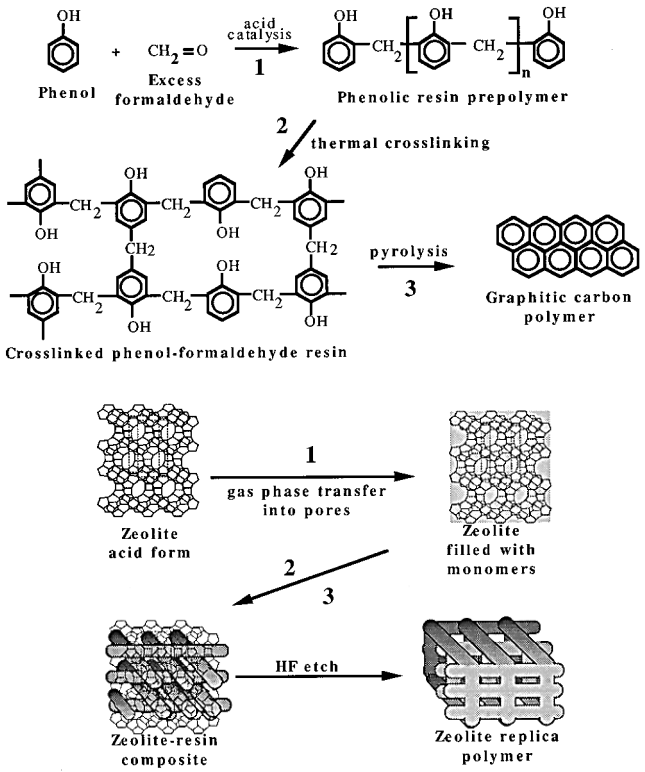

Figure 1. Schematic representation of the phenol−formaldehyde polymerization, cross-linking, and pyrolysis reactions, and the sequence of reaction steps used to prepare zeolite−resin composites and replica polymers.

impressively high surface areas.[12] In this paper we report the replication of zeolites using a thermoset phenol-formaldehyde resin (popularly known as Bakelite).[13] This polymer was chosen as an initial test case, because of two advantageous features. First, the two monomers can be transferred in the gas phase, and so the filling of the pores by each can be easily controlled. Second, the resulting polymer is heavily cross-linked, and therefore there is a reasonable expectation that the replica structure can be preserved upon template removal. However, because the resin forms in a condensation reaction, shrinkage is expected during polymerization. The pyrolysis reaction of the resulting phenolic resin, to produce a porous carbon material, is also expected to incur a further volume loss in the replica network.

Figure 1 illustrates the intrazeolitic polymerization reaction and the procedure by which the zeolite is removed to leave a replica. After the monomers are loaded into the solid, the acid-catalyzed polymerization reaction occurs, and the zeolite template is then dissolved away with aqueous hydrofluoric acid. The zeolites used in this study all have similar compositions, and contain pores defined by 12-rings of approximately 7 Å diameter, but each of them has a different channel topology.[14] Zeolites β and Y both have three-dimensionally interconnected pores. The channels in zeolite β are straight and intersect at right angles, while those in zeolite Y zigzag and intersect at tetrahedral angles. The channels in zeolite L are straight and do not intersect at all on the length scale of the phenol monomer. An interesting question, still remaining to be addressed after the initial demonstration of the technique by Kyotani et al.,[12] is the extent to which the template pore structure can be faithfully reproduced by replication. We report here that replication on the nanometer length scale of zeolite channels results in microporous polymers and carbons. The process does not preserve the crystalline order of the parent zeolite; nevetheless, the pore size distribution suggests that the process can be described as replication, because the majority of pores have the same dimensions as the zeolite wall. Furthermore, we report that chemically similar but topologically different templates produce polymer replicas with quite different microscopic structures and therefore different macroscopic physical properties.

Experimental Section

Materials. Zeolite Y (LZ-Y-72, Linde Y) and zeolite L (ELZ-L, Linde Type L) were obtained from Union Carbide Corp. in the sodium ion form. Zeolite β was synthesized using the procedure described by Perez-Pariente et al.,[15] using as received tetraethyl orthosilicate, 98%; tetraethylammonium hydroxide, 35% w/w, potassium hydroxide (all from Aldrich), sodium hydroxide, and sodium aluminate (both from EM Science). Reagent grade phenol, ammonium chloride (both from Fisher Scientific), paraformaldehyde, 95% w/w, and 48% HF (both from Aldrich) were also used as received. Purified water was obtained at 18.3 MΩ cm from a Barnstead Nanopure (SYBRON) system. Ultrahigh-purity N_2 gas (99.9995%, Scott Specialty Gases) was used in the gas adsorption measurements.

Synthesis of Polymer Resins and Polymer/Zeolite Composites. The polymerization of phenol and formaldehyde proceeds via an acid-catalyzed condensation reaction. To provide such an environment in the solid state, the zeolites were each ion exchanged with excess 1 M NH_4Cl for a total of 3 days, filtering and adding them to a fresh salt solution each day. The ammonium ions were decomposed at 500 °C in air to produce Brønsted acid sites in the zeolite. The zeolite samples were transferred in a drybox to the reaction flask and dried under vacuum at 125 °C for 5 h prior to the introduction of organic monomers. TGA analyses showed that the water content of the zeolites was 5−10% following this low-temperature drying step. Solid phenol was added to the flask and incubated with the acid zeolite at 65 °C under reduced pressure overnight. The amount of phenol incorporated was determined by the pore volume of the dehydrated acid zeolite (0.26 g/g of zeolite Y, 0.21 g/g of zeolite β, and 0.11 g/g of zeolite L). Excess solid paraformaldehyde (0.21 g/g of zeolite Y, 0.17 g/g of zeolite β, and 0.91 g/g of zeolite L) was heated to 120 °C, to liberate monomeric formaldehyde, which was transferred as a gas to the phenol/zeolite composite. An immediate reddening of the solid indicated the initiation of the polymerization reaction. The samples were heated at 1 °C/min to a curing temperature of 125 °C and held at this temperature for 5 h in flowing argon in order to cross-link the polymer. The temperature was than ramped at 5 °C/min to 500 or 900 °C and the resin/zeolite composite, still under flowing Ar, was pyrolyzed for 14 h. The samples were then shaken in concentrated hydrofluoric acid

(7) (a) Martin, C. R. *Science* **1994**, *266*, 1961. (b) Martin, C. R. *Acc. Chem. Res* **1995**, *28*, 8, 61. (c) Martin, C. R. *Chem. Mater.* **1996**, *8*, 1739. (d) Lakshmi, B. B., Korhout, P. K.; Martin, C. R. *Chem. Mater.* **1997**, *9*, 857.
(8) Nicholls, I. A., Anderson, L. I., Ekberg, B. *Trends Biotechnol.* **1995**, *13*, 47.
(9) Wulff, G., Poll, H.-G.; Minarik, M. J. *Liq. Chromatogr.* **1986**, *9*, 385 and references therein.
(10) Dhal, P. K.; Arnold, F. H. *J. Am. Chem. Soc.* **1991**, *113*, 3, 7417.
(11) Enzel, P.; Bien, T. *Chem. Mater.* **1992**, *4*, 819.
(12) Kyotani, T., Nagai, T., Inoue, S.; Tomita, A. *Chem. Mater.* **1997**, *9*, 609.
(13) Wadlinger, R. L., Kerr, G. T., and Rosinske, E. J. U.S. Patent No. 3,308,069, 1967.
(14) Meier, W. M., Olson, D. H., Baerlocher, Ch. In *Atlas of Zeolite Structure Types*; Rees, L. V. C., von Ballmoos, R., Eds.; Elsevier Press: London, 1996; pp 62−63, 104−105, 132−133.
(15) (a) Perez-Pariente, J., Martens, J. A., Jacobs, P. A. *Appl. Catal.* **1987**, *31*, 35. (b) Perez-Pariente, J., Martens, J. A., Jacobs, P. A. *Zeolites* **1988**, *8*, 46.

overnight and filtered to leave the organic replica materials. Ashing analysis of the products consistently gave compositions with less than 2% residual aluminosilicate.

It should be noted that the phenol−formaldehyde condensation reaction requires acid or base catalysis, and no reaction was observed at ambient temperature when zeolites Y and L were used in alkali (Na^+ or K^+) forms. A bulk phenol−formaldehyde resin sample was prepared in the absence of zeolites for comparison purposes, by condensing formaldehyde vapor and anhydrous HCl onto phenol powder. This material was subjected to the same curing cycles and was treated with anhydrous HF under the same conditions as the zeolite−resin composites.

Characterization. Adsorption isotherms were measured by N_2 gas adsorption at −196 °C using a Micromeritics ASAP 2010 analyzer equipped with a 1 Torr transducer for micropore analysis. Approximately 100−400 mg of each sample was used for the analysis. The samples were evacuated at 200 °C for at least 4 h and until no further outgassing was observed. To obtain the adsorption isotherm, nitrogen gas was dosed onto the sample in increments of 3 mL/g of solid for data points below 0.03 P/P_0, and 10−15 more data points were obtained above this relative pressure from doses entered in a pressure table. Measurements were taken after the pressure was allowed to equilibrate within 5% variation. Surface area, pore size distribution, and pore volume were determined from the isotherms using the DFT Plus data reduction software.[16]

Powder X-ray diffraction (XRD) patterns were collected with a Philips X'Pert-MPD diffractometer equipped with Cu Kα radiation. Elemental analyses (carbon, hydrogen, and inorganic residue after combustion in an oxygen atmosphere at 1000 °C) were performed by Atlantic Microlabs. Scanning electron microscopy (SEM) was performed on a JEOL-JSM 5400 microscope at the Electron Microscope Facility for the Life Sciences in the Biotechnology Institute at Pennsylvania State University. The samples were attached to SEM sample stubs and coated twice with Au−Pd using a BAL-TEC SCD 050 sputter coater.

Infrared spectra were obtained in transmission mode, as KBr pellets, on a Perkin-Elmer FTIR spectrometer. The electronic conductivity of the replicas was determined qualitatively using a ceramic pellet die. The replica powder (10 mg) was held between a metal base and a metal rod, and approximately 200 pounds of pressure was applied. A Cole Palmer 1559-72 multimeter was used to measure the two-point dc conductivity of the replicas.

Results

Three types of replicas were made from each of the zeolites templates. In these three preparations, the number of pore filling/polymerization cycles and the curing temperatures were varied. In the first set, the zeolites were filled once with monomers and the composite was heated at 500 °C prior to etching with aqueous HF. Zeolite−resin composites and the corresponding replicas from this set are hereafter referred to as X1−500 (X = Y, β, or L and refers to the zeolite used). A second set, in which two cycles of pore filling and curing at 500 °C were conducted prior to etching, are denoted X2−500. To study changes induced by pyrolysis of the resin in the zeolite channels, a third set, X1−900, in which the composite was cured at 900 °C before removal of the template, was prepared.

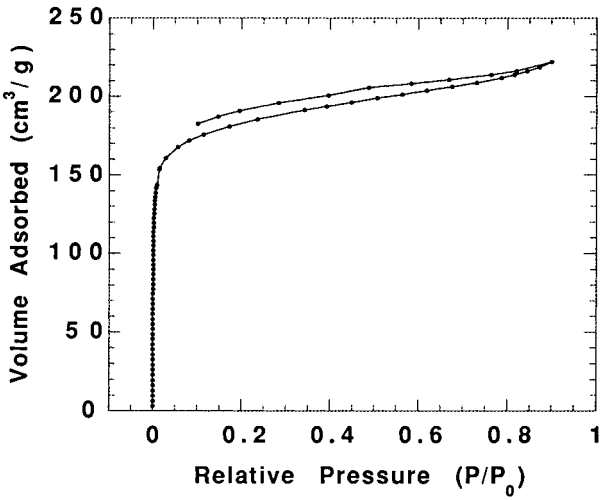

Figure 2. Nitrogen adsorption/desorption isotherms for the β2−500 replica polymer.

The change in micropore volume of the zeolites upon monomer loading and polymerization was followed in order to determine the extent to which the channels were filled by the resin. The micropore volumes of zeolite Y and β decreased by 80% after the monomers were loaded and cured. Evaporation of monomers and/or loss of mass from the condensation reaction accounts for the residual microporosity of these X1−500 composites. A second loading/curing cycle (X2−500 samples) was carried out in order to fill the remaining volume with the appropriate amount of phenol and formaldehyde. There was no detectable micropore volume in the twice-filled zeolite−resin composites. The micropore volumes of the once-filled zeolite−resin composites cured at 900 °C, prior to template removal, were approximately 40% those of the parent zeolites. The persistence of micropore volume in these samples is probably due to further loss of mass from the resin at higher temperatures, as mass is lost as small molecules, e.g., CO, CO_2, or water. Zeolite L samples cured at 500 °C were filled and cured only once (L1−500) since there was no observable micropore volume in these composites prior to etching with HF.

Nitrogen Adsorption. Figure 2 shows a typical nitrogen adsorption/desorption isotherm for a zeolite polymer replica sample. The isotherm shows two features −the rapid rise near zero pressure, and the adsorption/desorption hysteresis at higher pressure−that are typical of microporous materials. Adsorption data for all samples were analyzed quantitatively using the density functional theory (DFT) approach, which allows one to determine the surface area, pore volume, and pore size distribution from nitrogen adsorption isotherms.[16] Briefly, the DFT theory models the physical adsorption process at the fluid−solid interface as the adsorbing gas condenses at the surface of a solid. Density profiles are calculated over a range of relative pressures that reflect the density of the gas with distance from the surface. The density profiles are correlated to pore size, and by fitting the experimental isotherm to a set of density profiles, a pore size distribution is obtained.

The surface areas and micropore volumes of the replicas produced by HF etching of the zeolites are listed in Table 1. The replicas made by etching zeolites Y and

(16) (a) Olivier, J. P.; Conklin, W. B. Determination of Pore Size Distribution from Density Functional Theoretic Models of Adsorption and Condensation within Porous Solids. Presented at the *International Symposium on the Effects of Surface Heterogeneity in Adsorption and Catalysis on Solids*; Kazimier Dolny, Poland, July 1992. (b) Olivier, J. P.; Conklin, W. B.; Szombathely, M. V. Determination of Pore Size Distribution from Density Functional Theory: A Comparison of Nitrogen and Argon Results. In *Characterization of Porous Solids. Proceedings of the IUPAC Symposium (COPS III)*; Elsevier Press: Marselle, France, 1993. (c) Olivier, J. P. *J. Porous Mater.* **1995**, *2*, 9. (d) Olivier, J. P. *Fifth International Conference on the Fundamentals of Adsorption*, Pacific Grove, CA, 1995.

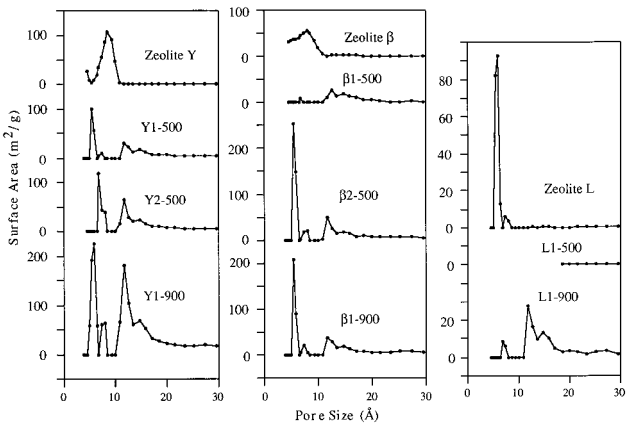

Figure 3. Pore size distribution plots of the replicas of (a) zeolite Y, (b) zeolite β, and (c) zeolite L.

Table 1. Elemental Analysis, Surface Areas, and Pore Volumes of the Template Zeolites and Corresponding Replicas

sample	surface area (m^2/g)	pore vol (mL/g)	replica C/H
zeolite Y	488	0.23	
Y1−500	320	0.18	2.17
Y2−500	479	0.31	2.38
Y1−900	1580	0.83	3.05
zeolite β	475	0.19	
β1−500	167	0.09	1.91
β2−500	604	0.29	2.00
β1−900	641	0.33	4.01
zeolite L	205	0.10	
L1−500	0.5	0.00	2.03
L1−900	121	0.10	2.70
bakelite	8	0.00	2.05

β that had been filled and cured once (Y1−500 and β1−500) had pore volumes and surface areas that were slightly lower than those of the parent zeolites. The replicas extracted from the composites that had been filled twice, however, had larger pore volumes and surface areas. The resins cured at 900 °C had an even higher degree of porosity, and in the case of the zeolite Y replica, almost 4 times that of the parent zeolite. This result is consistent with the high surface areas obtained at high polymerization temperature by Kyotani et al.[12] The zeolite L1−500 replicas were completely nonporous and had low surface areas, whereas L1−900 replicas had a surface area and pore volume nearly equal to that of the parent zeolite. It was found by X-ray diffraction (see below) that the acid form of zeolite L is not stable at 900 °C, so the porosity in this replica is probably not a direct result of template effects.

When the surface area that each pore size contributes to the total surface area is considered, all the replica polymers appear very similar. Figure 3 shows the pore size distributions. Each of the replicas has a bimodal distribution of pores, except of course the L1−500 replica, which is nonporous. Almost all of the porous replicas have a sharp peak in the distribution centered around 5−6 Å and a broader distribution between 12−30 Å. The relative amounts of the smaller and larger pores vary with preparation conditions. In particular, pyrolysis at 900 °C appears to favor the larger pores. The zeolite β replicas have the highest fraction of small pores, followed by the zeolite Y replicas.

Powder X-ray Diffraction. The X-ray diffraction (XRD) patterns of the host zeolites, zeolite−resin composites, and extracted replicas are shown in Figure 4. The microcrystalline zeolites have distinct diffraction patterns consisting of narrow Bragg peaks. The diffraction patterns of all the zeolite-resin composites cured at 500 °C were identical with those of the zeolite templates. Each of the zeolite−polymer composites responded differently to pyrolysis at 900 °C. The XRD pattern of the zeolite β composite did not change perceptibly upon heating to 900 °C, whereas the crystallinity in the zeolite Y material decreased noticeably, and that of the zeolite L composite was completely destroyed.

X-ray diffraction patterns of the replicas are quite different from those of the parent zeolite. There is no evidence in these patterns of the periodicity of the template, and the replicas are therefore best described as glassy or disordered. Broad diffraction features centered at 25−26° 2θ, corresponding to the stacking of carbon sheets, are evident in all the replica patterns. Because these broad features are not observable in the zeolite−resin composite prior to etching, it follows that they arise from partial collapse of the replica during the etching process.

Elemental Analysis and Infrared Spectroscopy. Elemental analysis revealed a C/H ratio near 2.0 for all the replicas cured at 500 °C. The same ratio was found for bulk phenol−formaldehyde resin heated at the same temperature under Ar, and is intermediate between the 1.17 calculated for the cross-linked polymer in drawn Figure 1 and a graphitic carbon. C/H ratios of individual replica polymers range from 1.91 to 2.38 and are listed in Table 1. The replica polymers prepared at 900 °C have higher C/H ratios, ranging from 2.70 for L1−900 to 4.01 for β1−900. These values are consistent with further condensation of the aromatic polymer to produce graphene ribbons and/or sheets.

Infrared spectra of zeolite Y resins and replicas (Figure 5) also illustrate the progress of the polymerization and curing reactions. The zeolite−resin composite before curing shows a strong absorption band at 808 cm^{-1}, which can be attributed to the out-of-plane C−H deformation of 1,2,6-disubstituted phenolic rings.[17] Apparently, the polymer is primarily linear at this stage, and remains so during the 500 °C curing step, although loss of OH groups is evident in the spectrum of the cured composite. Cross-linking at the 4-position of the phenol rings is evidenced by the appearance of a band at 897 cm^{-1}. This band appears, along with graphitic C−C stretching bands at 1590 and 1350 cm^{-1}, only when the zeolite is removed by etching with HF. The composite cured at 900 °C shows predominantly the graphitic bands, and less of the C−H deformation, the latter being predominantly from the cross-linked polymer. There is also a strong peak in the OH stretching region, indicating the presence of adsorbed water in these air-equilibrated samples.

Electron Microscopy. Figures 6 and 7 show transmission electron micrographs (TEM) of thin sections of the replica polymers. Figures 8−10 show scanning electron micrographs (SEM) of the zeolite crystallites and corresponding replicas. While neither the TEM nor the SEM instrument has sufficient resolution to image the channel structure of either the template or the replica, they do show the degree to which crystallite size and shape are preserved in the replication process.

In TEM images of replicas made from zeolites Y and β and cured at 500 °C, the particle morphology re-

(17) Hummel, D. O. *Infrared Analysis of Polymers, Resins, and Additives: An Atlas*; Wiley-Interscience: New York, 1971; Vol. I, Part 1, pp 115−124.

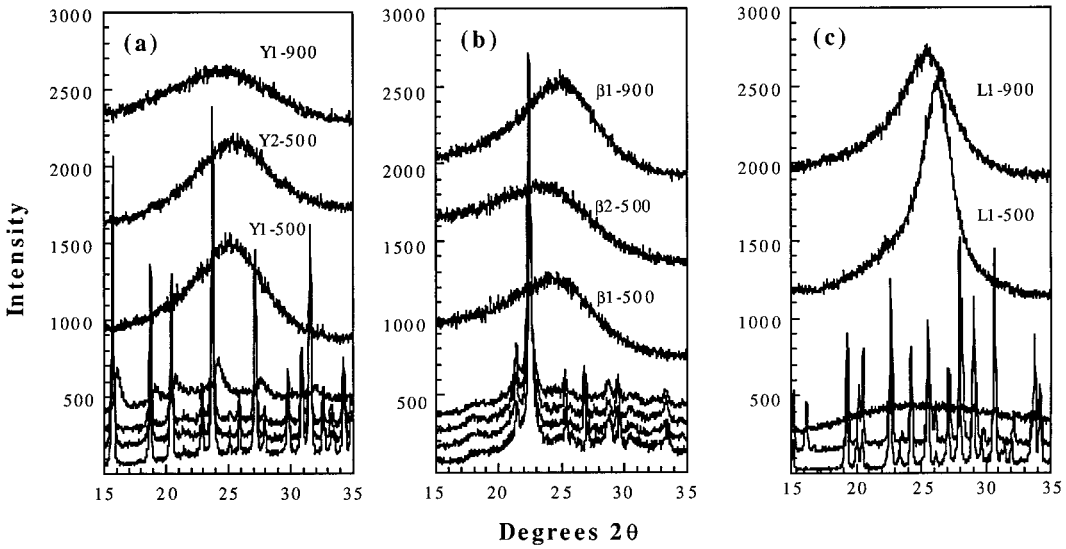

Figure 4. Ambient temperature powder XRD patterns of the zeolites, zeolite-resin composites, and replicas of (a) zeolite Y, (b) zeolite β, and (c) zeolite L. From the bottom, the plots in (a) and (b) are diffraction patterns of the zeolite, the X1−500 composite, the X2−500 composite, the X1−900 composite, and the corresponding replicas in the same order. The patterns in plot (c) are, from the bottom, zeolite L, the L1−500 composite, the L1−900 composite, and the corresponding replicas.

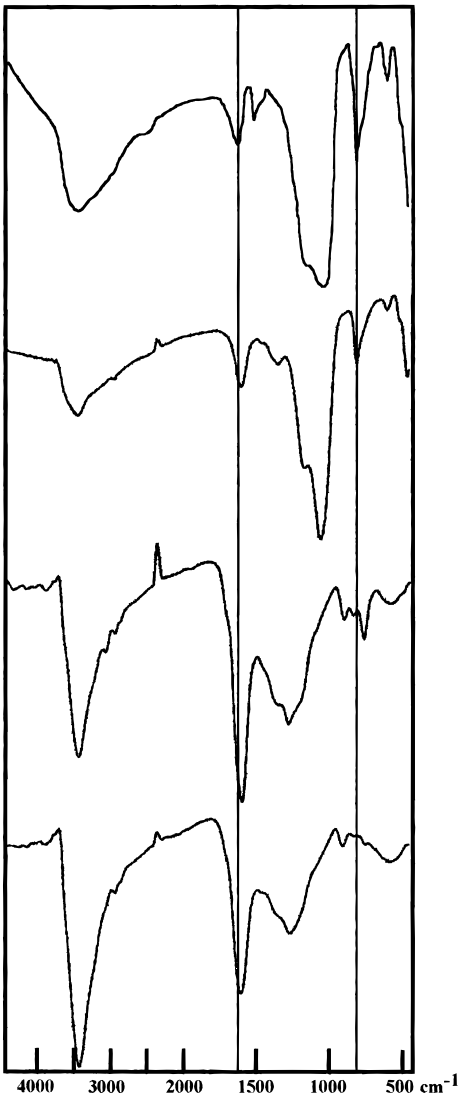

Figure 5. Infrared spectra of zeolite Y−resin composites and replicas. From the top, the plots are spectra of the uncured Y1 zeolite−resin composite, the Y2−500 composite, the Y2−500 replica, and the Y1−900 replica.

sembles that of the parent zeolite crystals. There are clearly observable void spaces in the center of the particles, showing that filling of the crystal is incomplete, even with two filling/curing cycles. These voids persist in the zeolite Y replica cured at 900 °C but do not appear in the zeolite β replica cured at the same temperature, suggesting that the polymer may flow during the high-temperature curing step in zeolite β. In constrast, the zeolite L "replicas" contain no voids and do not have discernible particle shapes that resemble the parent material. SEM images are consistent with the thin section TEM images. Replicas made from zeolites Y and β are morphologically very similar to the template materials, although some coalescence of grains is apparent in the β1−900 micrograph. The Y1−900 sample is indistinguishable in form from zeolite Y, indicating that the replica polymer is rigid enough to retain the shape of the particles even when partial destruction of the framework occurs at 900°C. In contrast, changes in form are very evident in the zeolite L samples. While there are some roughly spherical shapes that may represent the remnants of crystallites in the replica micrographs (Figure 10), the surface of the material is very highly textured, and no crystal faces or edges of the template zeolite are preserved.

Discussion

The total pore volumes and pore size distribution plots (Table 1 and Figure 3) of the zeolite templates, the zeolite−resin composites, and the polymer replicas support the notion of channel replication, as sketched in Figure 1. The process begins with a microcrystalline, high surface area zeolite, which has in every case a sharp distribution of <10 Å diameter micropores. The polymerization of phenol and formaldehyde in the channels dramatically reduces the pore volume, to essentially zero after two filling and curing cycles. In the case of zeolites Y and β, the pore volume is recovered when the aluminosilicate template is removed with HF. A bulk resin sample, prepared under the same conditions but without the zeolite template, has no detectable microporosity at any point in the reaction sequence.

The smaller micropores generated by replication of zeolites Y and β correspond closely to the 6 Å width of the zeolite walls that enclose the pore networks. A

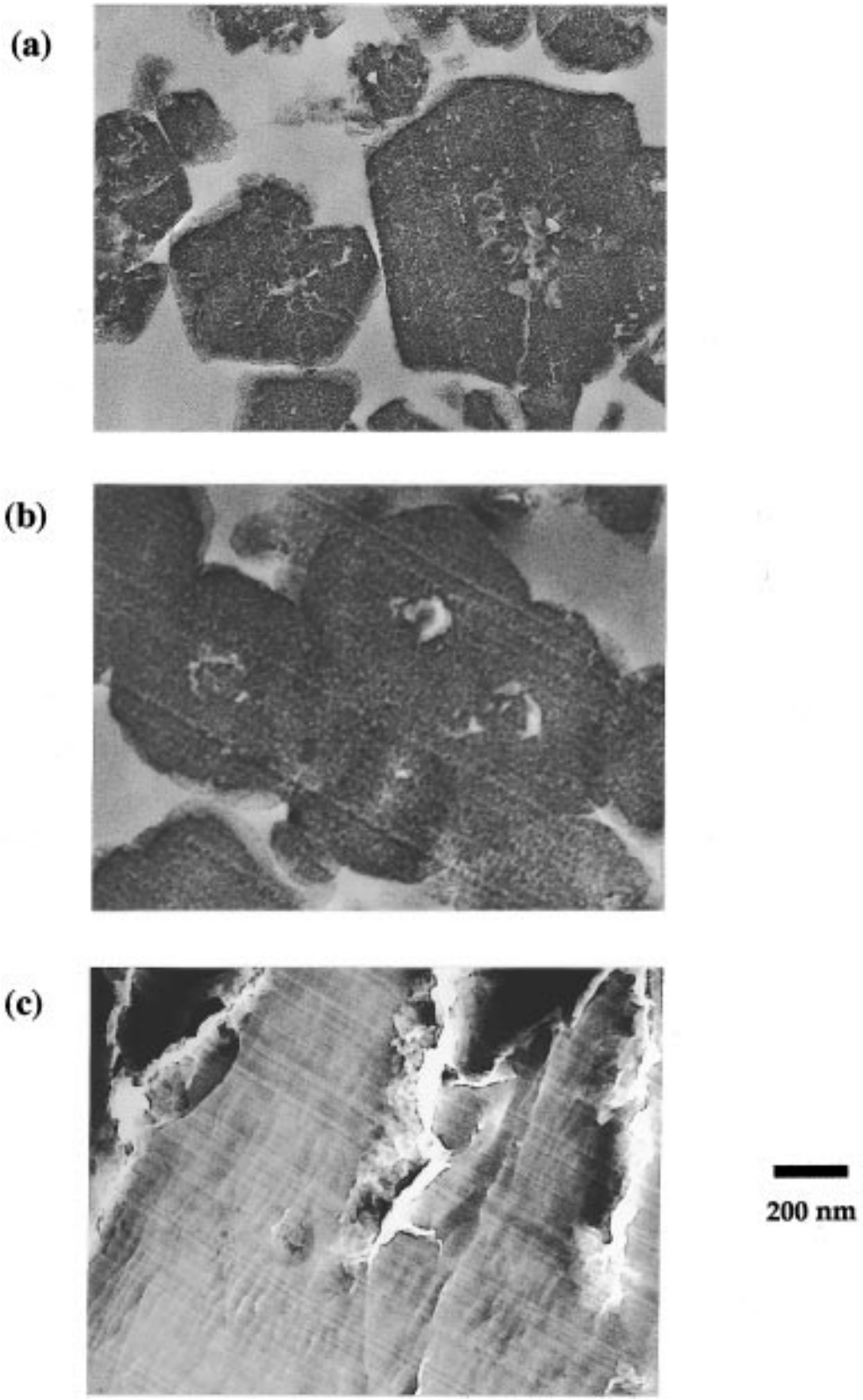

Figure 6. TEM images of thin sections of replicas (a) Y2−500, (b) β2−500, and (c) L1−500.

broader distribution of 12−30 Å pores is also present in all of the porous replicas. Doubling of pore widths is expected as a consequence of local collapse events, in which pairs of flanking cavities coalesce, and this effect may account for the peak in the micropore distributions around 12 Å. Another possible mechanism for the formation of larger micropores is the loss of mass from the replica within the channels of the template, which occurs during the course of condensation and pyrolysis reactions. Contraction of polymer will cause necking and discontinuities in the zeolite pores, and these features will remain when the template is removed. In the resulting discontinuous replica network, pores corresponding to the width of an unfilled zeolite channel or cage (ca. 12 Å) plus the two flanking walls (6 Å each) might be obtained. A distribution of 20−30 Å micropores is present in all the replica polymers and may be accounted for by this effect. Interestingly, the Y and β replicas made by filling the zeolites twice have greater micropore volumes than the once-filled samples. We

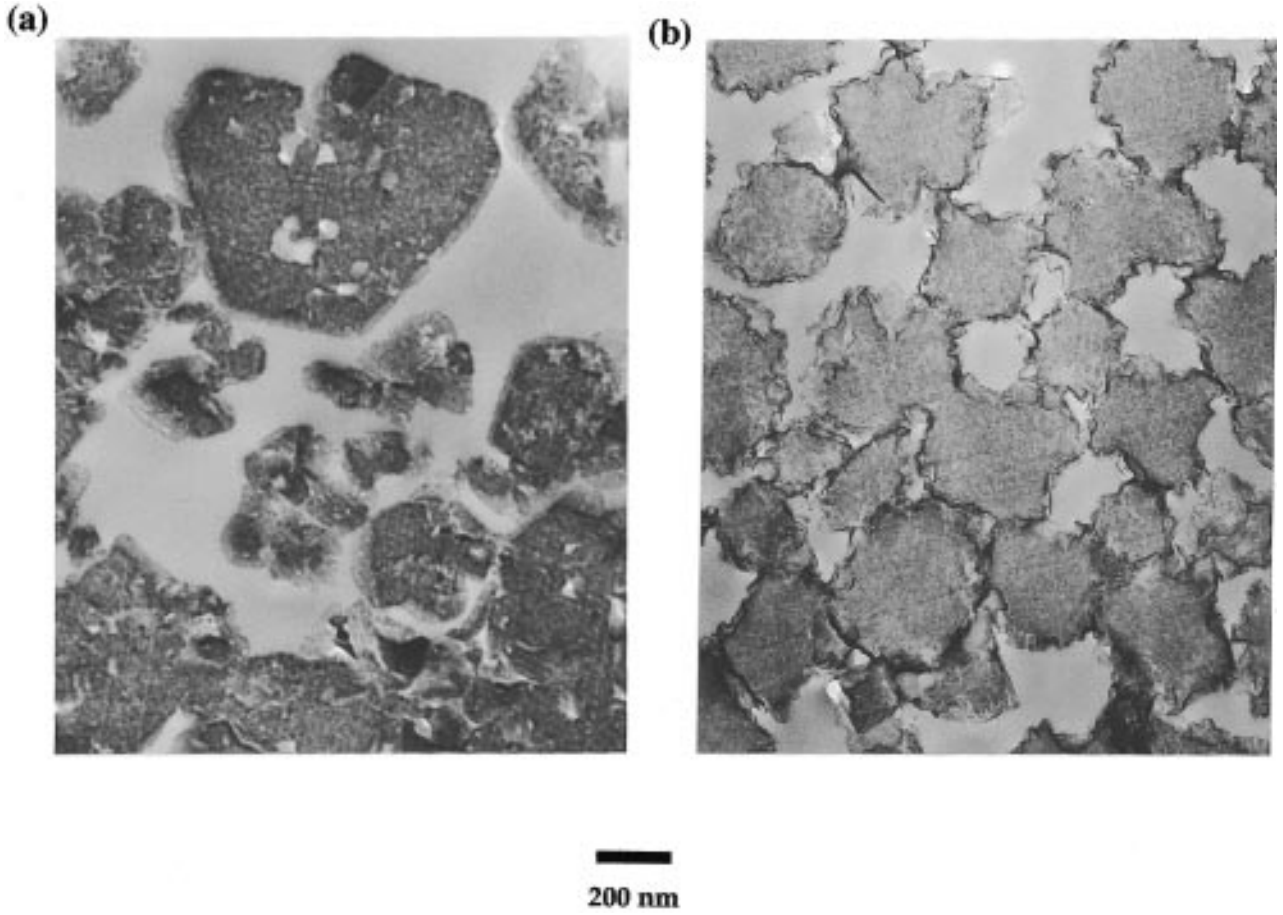

Figure 7. TEM images of thin sections of replicas (a) Y1−900 and (b) β1−900.

tentatively ascribe this to a higher degree of pore collapse in the once-filled replicas.

A rather striking difference in porosity is found between replicas made from different templates. Zeolites Y and β yield microporous replicas, whereas zeolite L gives a dense material. These differences may be understood by considering the channel topology of the zeolites, which is sketched in Figure 11. In the case of zeolites Y and β, the channels are interconnected in a three-dimensional network, and removal of the template leaves a free-standing, three-dimensional porous solid. In zeolite L, however, the channel interconnections consist of small cancrinite cages, which are inaccessible to the monomers that compose the replica polymer. Effectively, zeolite L has a one-dimensional channel structure, the replica of which is a set of polymer rods. Because of shrinkage in the condensation reaction, these rods will be discontinuous, and the material should therefore readily collapse upon removal of the aluminosilicate. In essence, the absence of interconnects that support a three-dimensional structure is responsible for the collapse of the pore volume in the L1−500 sample.

Considerable porosity is evident in the L1−900 replica, and this result seems strange in light of nonporosity of the L1−500 replica. This high porosity may be understood in terms of the stability of the proton-exchanged zeolites at 900 °C. Zeolite β, which is a high-silica zeolite, retains its crystallinity under these conditions. Zeolite Y shows partial loss of crystallinity, as evidenced by decreasing intensity of Bragg diffraction peaks. In the case of zeolite L, which has the lowest Si/Al ratio, and the L1−900 composite, X-ray diffraction patterns show that the crystallinity of the zeolite is lost at 900 °C. In this sample, the replica is cured as part of an amorphous alumina-silica composite. The L1−900 replica therefore has an opportunity to forge connections between rods prior to removal of the aluminosilicate.

X-ray diffraction patterns of the template zeolites, zeolite−resin composites, and replicas (Figure 3) show that the long-range order of the template is not preserved by the replica polymers. Instead, broad diffraction features reminiscent of glassy carbon are observed. In amorphous carbons and crystalline graphite, ribbons or semiinfinite sheets of carbon atoms arranged in a hexagonal mesh stack perpendicular to the ring plane to produce a Bragg diffraction peak. The *d* spacing of this diffraction line (the 002 reflection in crystalline graphite) is 3.35 Å in graphite and increases as the stacking becomes more disordered.[18,19] The intrinsic width of the peak increases as the average number of sheets in a stack decreases. The apparent width also increases if the diffraction pattern represents a distribution of *d* spacings.

The pyrolysis of phenol−formaldehyde resins results in the destruction of the methylene cross-links to form aromatic clusters, which begin to order at high temperatures.[20] It has been reported that in bulk phenolic resins clustering of aromatic units begins at 450 °C and that resins heated at 900 °C are completely carbon-

(18) (a) Lachter, J., Henry, L. G., Bragg, R. H. *J. Appl. Crystallogr.* **1988**, *21*, 92. (b) Aladekomo, J. B.; Bragg, R. H. *Carbon* **1990**, *28*, 8, 897.

(19) Rao, A. M., Fung, A. W. P., Dresselhaus, M. S., Endo, M. *J. Mater. Res.* **1992**, *7*, 1788.

(20) Daley, M. A., Tandon, D., Economy, J.; Hippo, E. J. *Carbon* **1996**, *34*, 1191.

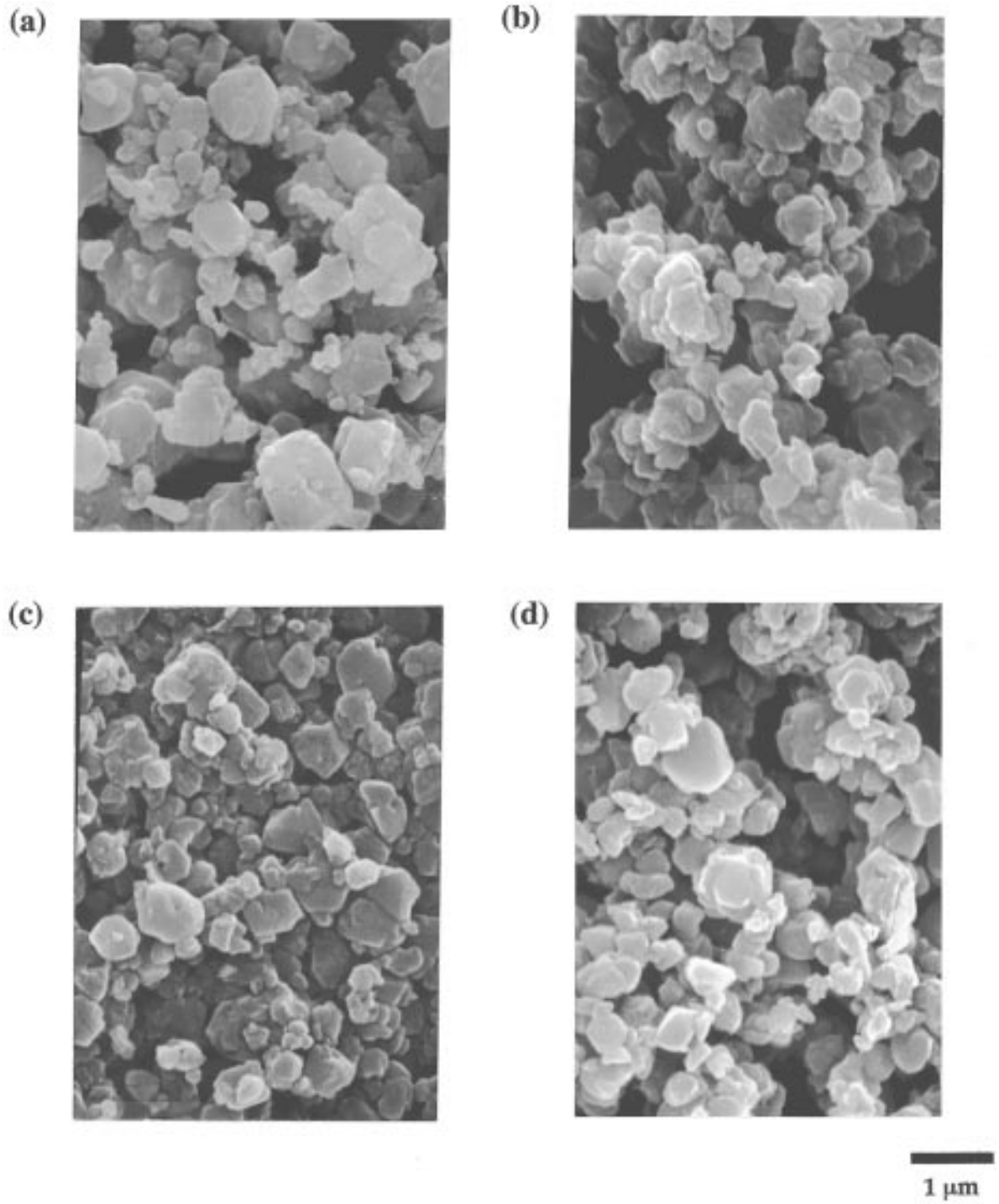

Figure 8. SEM images of (a) zeolite Y, (b) Y1−500 replica, (c) Y2−500 replica, and (d) Y1−900 replica. Scale bar is 1 μm.

ized.[21] The broad diffraction peak at 25−26° 2θ was absent in all of the zeolite−resin composites, but appeared in every case upon template removal by HF. This suggests that the aromatic units that form during the curing process are hindered from stacking in the confined spaces of the zeolite channels. However, upon removal of the template, partial collapse of the structure occurs to allow stacking of the sheets. To test this hypothesis, a control sample, in which the resin was synthesized on the surface of 50 nm spherical silica particles was prepared and cured. The glassy carbon diffraction peak was found in samples pyrolyzed at 500 and at 900 °C, indicating that the narrow channels were responsible for the absence of this peak in the zeolite−resin composites.

The appearance of this diffraction peak varies among the replicas made from zeolite Y, β, and L. In all the replicas produced from three-dimensional templates Y and β, it is broad, and centered at $d \approx 3.7$ Å. In contrast, the diffraction peak is sharper and appears at higher angle ($d = 3.52$ Å) in the L1−500 replica. In addition to peaks corresponding to the graphite (002) reflection, the pattern of the L1−500 replica also contains weak (004), (100), and (101) reflections at higher angles (not shown). This three-dimensional ordering of graphene ribbons in the L1−500 sample correlates with the surface area results and provides evidence that the unsupported replica collapses to a bulk

(21) Gupta, A.; Harrison, I. R. *Carbon* **1994**, *32*, 953.

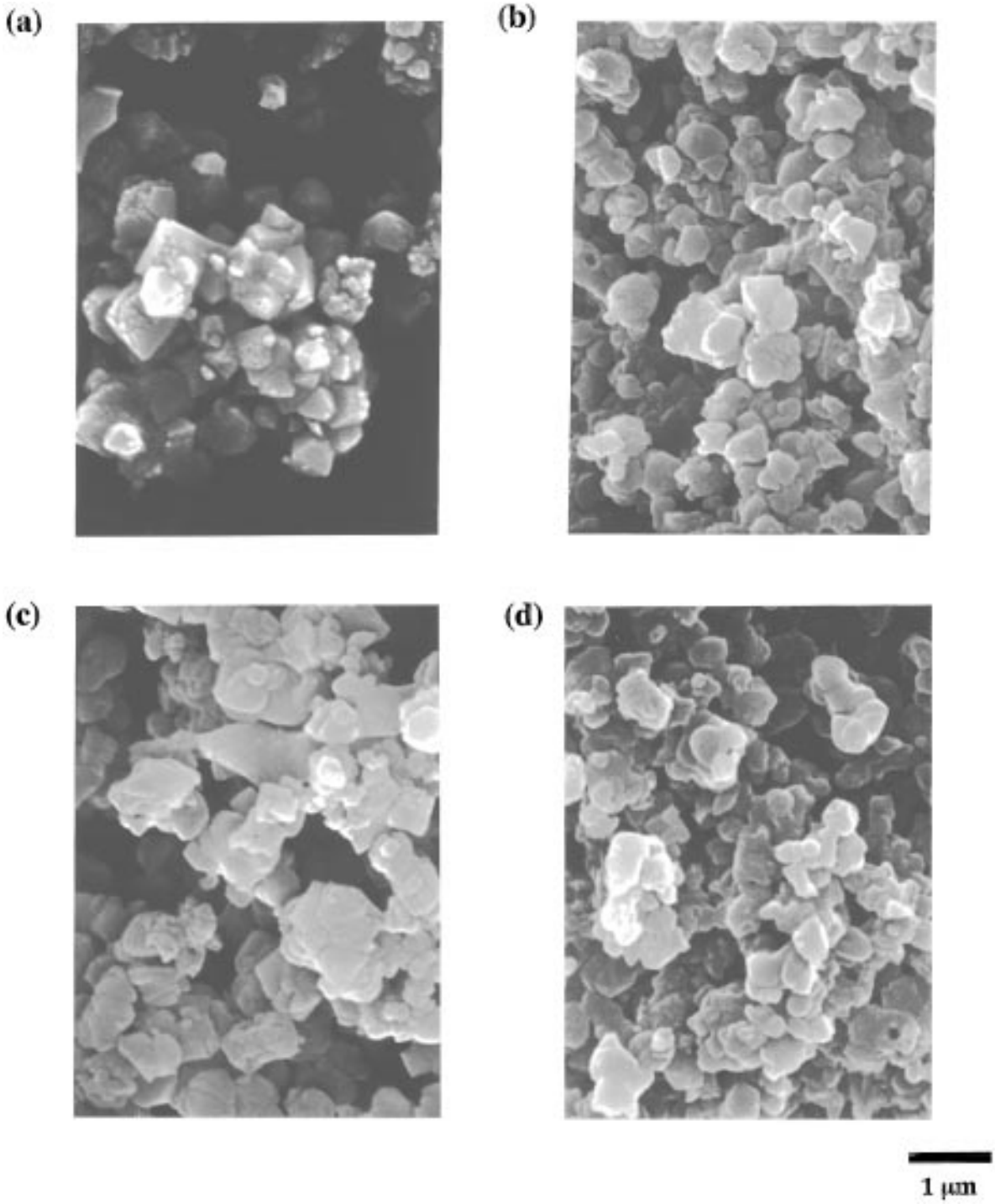

Figure 9. SEM images of (a) zeolite β, (b) β 1−500 replica, (c) β 2−500 replica, and (d) β 1−900 replica. Scale bar is 1 μm.

material upon removal of the aluminosilicate template. Interestingly, the L1−900 replica is intermediate in crystallinity between the high surface area, microporous replicas (from Y and β) and the L1−500 sample. Recall that the long-range order of the zeolite−resin composite is lost prior to template removal in this case. There are cross-links between channels that reinforce a porous microstructure in L1−900, and the same cross-links hinder the stacking of planes.

Elemental analysis results of the replicas processed at 900 °C (Table 1) are consistent with partial graphitization of the replica. A fully crystallized graphite sample should have a high C/H ratio, whereas that of a single hydrogen-terminated graphene ribbon (one ring wide and infinite in length) would be 2.0. The pyrolyzed replicas are intermediate between these extremes, ranging from 2.7 to 4.0. In the β1−900 and Y1−900 replicas, C + H represent about 90% of the sample. The aluminosilicate contents are <2%, implying a significant amount of oxygen (and/or fluorine) in the replicas. In L1−900, C + H amounts to only about 80% of the mass of the replica, the balance again being oxygen (and/or fluorine). Interestingly, the β1−900 replica has the highest C/H ratio, and L1−900 the lowest. C/H ratios much larger than 2.0 may arise from condensation of graphene ribbons at the interconnections of channels. We note that these interconnections predominate in the Y and β structures, but are absent in L.

Electron micrographs (Figures 6−10) corroborate the results of the porosity and XRD measurements. With three-dimensional replicas, both the size and shape of the parent crystallites are retained, even though over

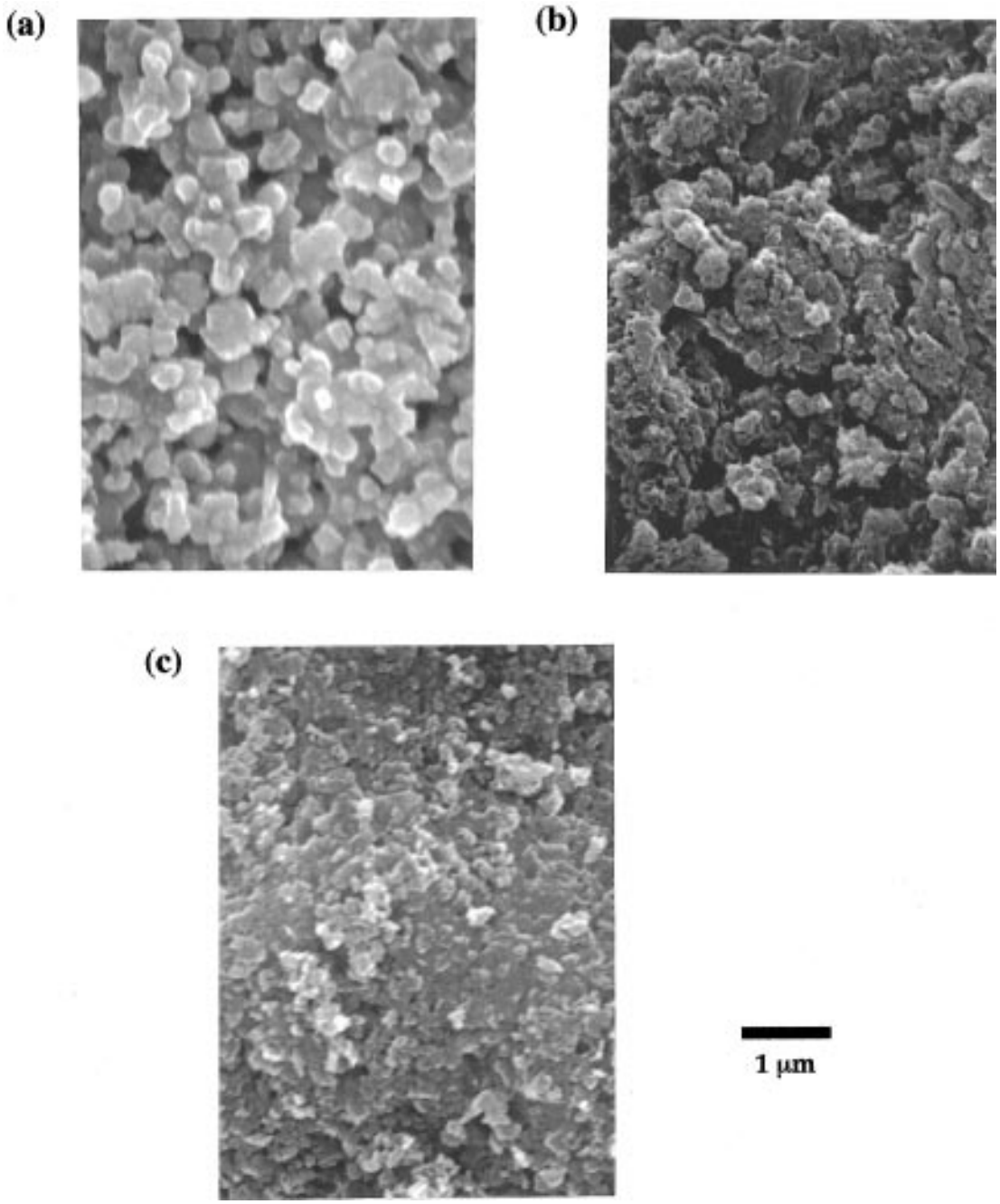

Figure 10. SEM images of (a) zeolite L, (b) L1−500 replica, and (c) L1−900 replica. Scale bar is 1 μm.

half of the mass of the zeolite−resin composite is lost when the aluminosilicate component is dissolved in HF. In the case of zeolite L, there is substantial rearrangement of the discontinuous polymer, which is revealed in the macroscopic morphological features of the replica.

Qualitative tests of the electronic conductivity of the pyrolyzed replicas were made in order to compare them to other conducting carbons. Carbon materials, such as glassy carbon, are conductive if there is enough organization and connectivity between carbon sheets and between individual grains in the case of powder samples. The electronic conductivity decreases as the material becomes more amorphous. Previous studies have shown that carbon fibers are more graphitic when treated at higher temperatures and undergo a phase transition at around 1200 °C.[22] This phase transition induces an increase of several orders of magnitude in the conductivity. Simple two-point conductivity measurements of compressed powders revealed significant differences in the conductivities of the X1−900 replicas. The conductivity of the zeolite L replica is about the same as that of powdered glassy carbon. Interestingly, the β1−900 replica, produced from a three-dimensional array of intersecting straight channels, is about 2 orders of magnitude more conducting. Zeolite Y, which has zigzag channels, produces a replica carbon that is about 5 orders of magnitude less conductive than the zeolite β replica. While these simple two-point dc conductivity measurements are only approximate and depend on such parameters as pressure and particle morphology, it seems unlikely that the very large difference between the Y and β replicas can be accounted for by these effects.

Note that the conductivity results do not correlate with the observed C/H ratios, i.e., Y1−900 has a C/H ratio intermediate between β1−900 and L1−900, but

(22) Kuriyama, K.; Dresselhaus, M. S. *M. Mater. Res.* **1992**, *7*, 940.

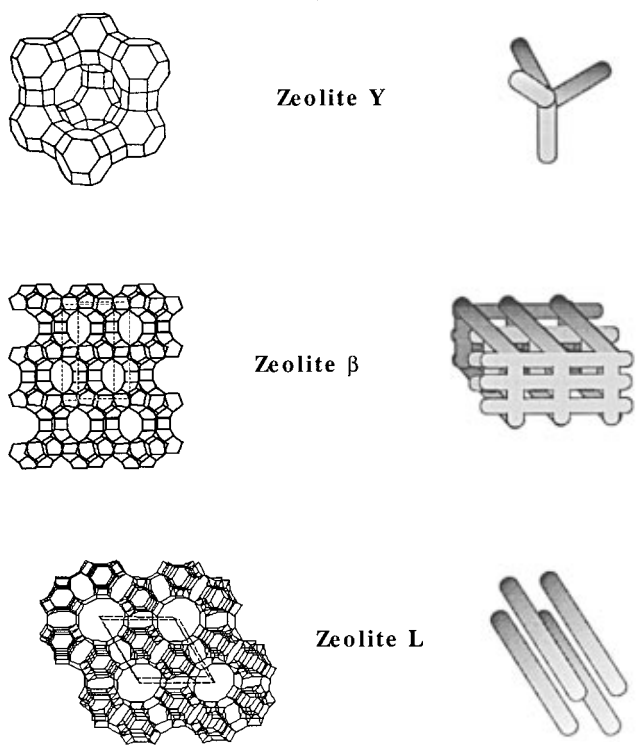

Figure 11. Schematic illustration of the frameworks and pore interconnections in zeolites β, Y, and L.

the lowest conductivity. The dramatic differences in conductivity appear to be better correlated with the topology of channel networks in the template zeolites. It has been reported in other studies that graphitization with the formation of extended sheetlike structures is not possible in zeolite Y for steric reasons.[11] We note that there are directions (e.g., 110) that allow a "straight shot" through the faujasite channel structure but that these pathways are not circular in projection and may not allow graphene ribbons to grow easily.

It is important to recall that contact resistance between grains may have an important effect on the overall conductivity of these samples, and the most faithful replication of crystallites (Y1−900) could lead to the highest contact resistance. However, this effect would not explain the difference between the L1−900 and β1−900 conductivities. We therefore tentatively attribute the observed differences in conductivity to the different channel architectures of zeolites Y, β, and L, although further verification of this concept, using replicas prepared from a variety of different template zeolites and mesoporous sieves, is needed.

Conclusions

The polymer replication of zeolites was studied using three different frameworks, which have similar composition and approximately the same channel dimensions but different pore network topologies. The three-dimensional, tetrahedrally interconnected channels of zeolite Y yield X-ray amorphous replicas with high surface areas and large micropore volumes. Replication of zeolite β also results in a microporous material with a distribution of pore diameters very similar to that of the zeolite Y replicas. The straight one-dimensional channels of zeolite L influence the intrazeolite polymerization chemistry, but cannot produce a free-standing porous replica, unless the processing temperature is sufficiently high to destroy the crystallinity of the template.

The extension of this technique to templates and replicas of different topologies and compositions is now being investigated. The aluminosilicates studied here require rather forcing conditions (aqueous HF or strong base) for template removal. However, other thermally stable, microporous materials, such as aluminophosphates, gallophosphates, and zincophosphates, can be decomposed under mild conditions. Replicas of these frameworks might be prepared from organic monomers or inorganic preceramic polymers with a much broader range of compositions and properties. In summary, the phenol−formaldehyde replica polymers described herein exemplify a new and possibly quite general method for synthesizing zeolitic materials. In choosing the templates for these syntheses, one should be aware that the topology of their pore networks can have important consequences in determining the macroscopic properties of the replicas.

Acknowledgment. This work was supported by a grant from the National Institutes of Health, GM-43844. Instrumentation for the X-ray diffraction experiments was provided by NSF Grant DMR-9402860. We also thank Dr. Rosemary Walsh for help in obtaining the SEM images.

CM9703278